

# Goodness-of-fit for amplitude analysis with anomaly detection

Guoyi Hou<sup>1,2\*</sup> and Bei Jiang Liu<sup>1,2</sup>

<sup>1\*</sup>Institute of High Energy Physics, Beijing, 100049, People's Republic of China.

<sup>2</sup>University of Chinese Academy of Sciences, Beijing, 100049, People's Republic of China.

\*Corresponding author(s). E-mail(s): [hougy@ihep.ac.cn](mailto:hougy@ihep.ac.cn);  
Contributing authors: [liubj@ihep.ac.cn](mailto:liubj@ihep.ac.cn);

## Abstract

Amplitude analysis serves as a pivotal tool in hadron spectroscopy, fundamentally involving a series of likelihood fits to multi-dimensional experimental distributions. While numerous robust goodness-of-fit tests are available for low-dimensional scenarios, evaluating goodness-of-fit in amplitude analysis poses significant challenges. In this work, we introduce a powerful goodness-of-fit test leveraging a machine-learning-based anomaly detection method.

**Keywords:** Goodness-of-fit, Amplitude analysis, Anomaly detection

## 1 Introduction

The strong force, governed by Quantum Chromodynamics (QCD), regulates the interactions between quarks and gluons, the fundamental constituents responsible for the majority of visible mass in the universe. A central challenge in QCD is elucidating the complex hadron spectrum in terms of quark and gluon degrees of freedom. The spectrum of both ordinary and exotic hadrons has been extensively explored in experiments such as BESIII, LHCb, and Belle II. Due to the short-lived nature of these hadronic states, information about resonances must be inferred from the kinematic distributions of their decay products. Amplitude analysis techniques are often employed, accounting for potential interferences among intermediate resonances and leveraging the full kinematic information embedded in the data [1]. For an n-body final state, a set of

3n–4 kinematic variables is required to fully define the decay kinematics. Quantum mechanical amplitudes yield a probability distribution and predict the distributions of final-state particles for a given process. To extract amplitude parameters, unbinned likelihood fits are performed on high-dimensional data.

Goodness-of-fit tests are a critical component of amplitude analyses, assessing the level of agreement between the fit model and the data. For one-dimensional problems, a variety of robust goodness-of-fit tests are available, such as the well-known  $\chi^2$  or Kolmogorov-Smirnov tests. Some of these can be extended to two or three dimensions if the sample size is sufficiently large. However, in high-dimensional settings, these tests rapidly lose power due to the “curse of dimensionality”, as finite samples become sparse in high-dimensional spaces [2]. A goodness-of-fit test can be effectively interpreted as a problem of determining whether two data samples are drawn from the same (unknown) statistical distribution. Machine learning (ML) classification was first proposed for multivariate goodness-of-fit and two-sample testing [3]. Various ML-based anomaly detection methods have been explored in high-energy physics to search for new physics beyond the Standard Model [5–9]. The goal is to identify discrepancies between experimental data, which may contain a mixture of background and potential signal events, and a reference background dataset. These binary classification procedures can be adapted for high-dimensional two-sample testing, with the classifier’s output distributions used to perform a univariate two-sample test.

In this work, we employ an ML-based anomaly detection method to evaluate goodness-of-fit for amplitude analyses. Anomalous data behavior is identified by comparing high-dimensional distributions between experimental data and Monte Carlo (MC) samples generated according to the amplitude analysis results. We construct a classifier using XGBoost [4] to detect localized anomalies in high-dimensional data. Statistical tests are developed using the probabilistic classifier’s output. We demonstrate the performance of this approach using the amplitude analysis of the multi-body decay process  $J/\psi \rightarrow \gamma 4\pi$  as an example. Additionally, goodness-of-fit is evaluated for various signal strengths and types of intermediate resonances. The ML-based anomaly detection approach demonstrates promising performance in testing goodness-of-fit for amplitude analyses.

## 2 Method

In amplitude analysis, an unbinned maximum likelihood fit of a probability density function (PDF) to an experimental dataset is performed. A common approach involves generating one-dimensional histograms, such as invariant mass and angular distributions, for the data and the projections of the fit model. These projections are obtained using an MC sample generated according to the amplitude analysis results. The  $\chi^2/n_{bin}$  for each one-dimensional distribution is used to assess goodness-of-fit, where  $n_{bin}$  is the number of bins in the histogram. The  $\chi^2$  is defined as  $\chi^2 = \sum_{i=1}^{N_{bin}} \frac{(n_i - \nu_i)^2}{\nu_i}$ , where  $n_i$  and  $\nu_i$  represent the number of events in the data and fit projections, respectively, for the  $i$ th bin of the distribution. However, this approach has limitations. First, it cannot account for correlations between distributions. Second, data become sparse as the dimensionality of the histograms increases.

Following the method proposed in Ref. [3], binary multivariate classification can be used to test whether two data samples are drawn from the same statistical model. An ML classifier is trained to discriminate between the MC sample generated from the amplitude analysis fit results and the experimental data based on high-dimensional observables. The classifier’s performance is then used to construct test statistics [8], such as the Likelihood Ratio Test (LRT) and Area Under the Curve (AUC). The AUC statistic measures the classifier’s ability to distinguish between the data and MC samples. Alternatively, the classifier estimates the density ratio between the data and MC distributions, which is used to construct test statistics such as the Likelihood Ratio Test (a Neyman-Pearson test). To test the null hypothesis—that the data and MC share the same distribution—the distribution of the test statistic under the null hypothesis must be known. Using the bootstrap method proposed in Ref. [8], we repeatedly resample the data and MC samples with replacement, recompute the test statistic for each resampled dataset, and use the distribution of these statistics to approximate the null distribution. The bootstrap method is flexible and does not rely on asymptotic approximations, making it suitable for high-dimensional data. To detect localized anomalies, p-values are calculated using the test statistics and their estimated null distributions. The p-value represents the probability of observing a test statistic indicating lesser agreement than the actual observed value under the null hypothesis. The workflow for this goodness-of-fit test approach is illustrated in Figure 1.

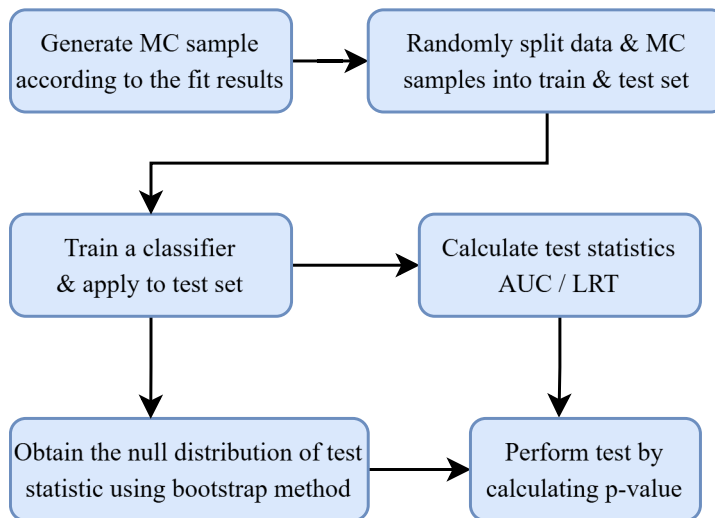


**Fig. 1** Workflow for the goodness-of-fit test approach using anomaly detection.

### 3 Anomaly detection using XGBoost

Given the dimensionality and size of the datasets for amplitude analysis, XGBoost (Extreme Gradient Boosting) [4] is a suitable algorithm for constructing the probabilistic classifier in this work. XGBoost is a highly efficient and scalable implementation of gradient boosting machines, widely used in various applications. Table 1 presents the configuration of XGBoost hyperparameters, determined through Bayesian Optimization [11, 12]. Key hyperparameters include: *eta* is the learning rate which controls the step size at each boosting iteration, and was optimized to 0.1. *max\_depth* limits the maximum depth of individual decision trees, which is optimized to 6. *min\_child\_weight* determines the minimum sum of instance weights required in a child node and was optimized to 5.0, further controlling tree complexity. *gamma* defines the minimum loss reduction required to make a further partition on a leaf node of the tree, controlling tree pruning, and was optimized to 0.1. *subsample* means the subsample ratio of training instances, was optimized to 0.8. Similarly, *colsample\_bytree*, the subsample ratio of columns when constructing each tree, was optimized to 1.0. *lambda*, the L2 regularization term, was optimized to 4.5, while *alpha*, the L1 regularization term, was set to 0.1. A 5-fold cross-validation is employed to improve generalization performance and reduce overfitting.

**Table 1** Configuration of XGBoost hyperparameters

Option	Configuration	Range	Description
objective	binary:logistic	-	Classification objective function
eval_metric	logloss	-	Evaluation metric
eta	0.1	0.01–0.3	Learning rate
max_depth	6	3–10	Maximum depth of the decision tree
min_child_weight	5.0	1.0–10.0	Minimum sum of instance weight needed in a child
subsample	0.8	0.5–1.0	Subsample ratio of the training instances
colsample_bytree	1.0	0.5–1.0	Subsample ratio of columns when constructing each tree
lambda	4.5	0.1–10.0	L2 regularization term
alpha	0.1	0.0–1.0	L1 regularization term
gamma	0.1	0.0–1.0	Minimum loss reduction required for a split

## 4 Experiments

### 4.1 Data description

We use the amplitude analysis of  $J/\psi \rightarrow \gamma\pi^+\pi^-\pi^0\pi^0$  process to demonstrate the performance of the goodness-of-fit test. The study of glueballs and hybrids is crucial for gaining insights into the gluon degree of freedom of the strong interaction at low energy scales, which is essential for understanding non-perturbative QCD. Hybrids and glueballs are expected to be abundantly produced in gluon-rich processes, such as  $J/\psi$  decays. The BESIII experiment, with its collection of 10 billion  $J/\psi$  events, provides

an ideal laboratory for exploring glueballs and hybrids. The  $J/\psi \rightarrow \gamma 4\pi$  process is of importance for the study of glueballs and hybrids. For  $J/\psi$  produced from  $e^+e^-$  annihilation, the final-state particles of the  $J/\psi \rightarrow \gamma 4\pi$  process can be represented in a 10-dimensional phase space, given the trivial integral over the rotation around the beam axis. In this work, we select invariant masses of eight pairs of final-state particles and two of the three Euler angles specifying the orientation of the final system relative to the  $e^+e^-$  as the coordinates of the 10-dimensional phase space for the  $J/\psi \rightarrow \gamma 4\pi$  process. Table 2 lists the kinematic observables used to represent the phase space.

**Table 2** Descriptions of the observables used to represent the phase space for  $J/\psi \rightarrow \gamma 4\pi$  process. In this table,  $\pi_1^0$  and  $\pi_2^0$  denote the  $\pi^0$  with higher and lower energy, respectively.

Observable	Description
$\cos\theta(X)$	Cosine of polar angle of X ( $4\pi$ ) in $J/\psi$ rest frame
$\phi_X(\pi^+)$	Azimuthal angle of $\pi^+$ in X helicity frame
$M(\pi^+\pi^-)$	Invariant mass of $\pi^+\pi^-$
$M(\pi^+\pi_1^0)$	Invariant mass of $\pi^+$ and $\pi_1^0$
$M(\pi^+\pi_2^0)$	Invariant mass of $\pi^+$ and $\pi_2^0$
$M(\pi^-\pi_1^0)$	Invariant mass of $\pi^-$ and $\pi_1^0$
$M(\pi^-\pi_2^0)$	Invariant mass of $\pi^-$ and $\pi_2^0$
$M(\pi_1^0\pi_2^0)$	Invariant mass of $\pi_1^0\pi_2^0$
$M(\gamma\pi_1^0)$	Invariant mass of $\gamma$ and $\pi_1^0$
$M(\gamma\pi_2^0)$	Invariant mass of $\gamma$ and $\pi_2^0$

## 4.2 Experiment setup

For demonstration purposes, we consider an amplitude analysis of experimental data searching for new resonances. The underlying physics of the experimental data is described by a specific set of amplitudes with intermediate resonances. If a resonance is missing in the fit model, discrepancies between the data and fit results will arise. We generate MC samples as pseudo-data using a set of amplitudes with intermediate resonances. Quasi-two-body amplitudes in the sequential radiative decay processes  $J/\psi \rightarrow \gamma X$ ,  $X \rightarrow Y\pi$ ,  $Y \rightarrow \pi Z$ ,  $Z \rightarrow \pi\pi$  are constructed using the covariant tensor amplitudes described in Ref. [10]. We validate the method across two distinct scenarios: Case 1, a subprocess  $J/\psi \rightarrow \gamma f_0(2100)$ ,  $f_0(2100) \rightarrow \pi \mathbf{a}_1(\mathbf{1260})$ ,  $a_1(1260) \rightarrow \rho\pi$ ,  $\rho \rightarrow \pi\pi$  is missing in the fit model, corresponding to an additional resonance in the  $3\pi$  spectrum,  $a_1(1260)$ . Case 2, a subprocess  $J/\psi \rightarrow \gamma \mathbf{f}_0(\mathbf{2100})$ ,  $f_0(2100) \rightarrow \pi a_1(1260)$ ,  $a_1(1260) \rightarrow \rho\pi$ ,  $\rho \rightarrow \pi\pi$  is missing in the fit model, corresponding an additional resonance in  $4\pi$  system,  $f_0(2100)$ . The sub-processes with intermediate resonances considered in these scenarios are detailed in Table 3. Event information at the generator level is used to produce the pseudo-data sample. The MC sample generated according to the fit model is compared to the pseudo-data sample to conduct the goodness-of-fit test. In all experiments, the pseudo-data set contains  $5 \times 10^5$  events, , each generated with a full set of four amplitudes listed in Table 3. The MC dataset also contains  $5 \times 10^5$  events, , each generated with a set of three amplitudes from Table 3.

**Table 3** The sub-processes with intermediate resonances included in MC or pseudo data set. The additional resonances are marked in bold. Case 1, a subprocess  $J/\psi \rightarrow \gamma f_0(2100), f_0(2100) \rightarrow \pi \mathbf{a}_1(1260), a_1(1260) \rightarrow \rho\pi, \rho \rightarrow \pi\pi$  is missing in the fit model, corresponding to an additional resonance in the  $3\pi$  spectrum,  $a_1(1260)$ . Case 2, a subprocess  $J/\psi \rightarrow \gamma \mathbf{f}_0(2100), f_0(2100) \rightarrow \pi a_1(1260), a_1(1260) \rightarrow \rho\pi, \rho \rightarrow \pi\pi$  is missing in the fit model, corresponding an additional resonance in  $4\pi$  system,  $f_0(2100)$ .

Sub-process	pseudo data set	MC set
<b>Case 1</b>		
$J/\psi \rightarrow \gamma\eta(1760), \eta(1760) \rightarrow \rho\rho, \rho \rightarrow \pi\pi$	✓	✓
$J/\psi \rightarrow \gamma f_2(2340), f_2(2340) \rightarrow \rho\rho, \rho \rightarrow \pi\pi$	✓	✓
$J/\psi \rightarrow \gamma f_0(2100), f_0(2100) \rightarrow \sigma\sigma, \sigma \rightarrow \pi\pi$	✓	✓
$J/\psi \rightarrow \gamma f_0(2100), f_0(2100) \rightarrow \pi \mathbf{a}_1(1260), a_1(1260) \rightarrow \rho\pi, \rho \rightarrow \pi\pi$	✓	×
<b>Case 2</b>		
$J/\psi \rightarrow \gamma\eta(1760), \eta(1760) \rightarrow \rho\rho, \rho \rightarrow \pi\pi$	✓	✓
$J/\psi \rightarrow \gamma f_0(1500), f_0(1500) \rightarrow \rho\rho, \sigma \rightarrow \pi\pi$	✓	✓
$J/\psi \rightarrow \gamma\eta_1(1855), \eta_1(1855) \rightarrow \pi a_1(1260), a_1(1260) \rightarrow \rho\pi, \rho \rightarrow \pi\pi$	✓	✓
$J/\psi \rightarrow \gamma \mathbf{f}_0(2100), f_0(2100) \rightarrow \pi a_1(1260), a_1(1260) \rightarrow \rho\pi, \rho \rightarrow \pi\pi$	✓	×

The signal strength  $\lambda$  is represented by the fraction of an intermediate resonance  $X$ , defined as  $\frac{\sigma_X}{\sigma}$ , where  $\sigma' \equiv \int |M(\xi)|^2 \Phi(\xi) d\xi$  and  $\sigma_X \equiv \int |A_X(\xi_i)|^2 \Phi(\xi) d\xi$ . Detection efficiency is assumed to be 100%, as the data samples are produced at the generator level. An event is characterized by the measured four-momenta of the final particles,  $\xi$ .  $\Phi(\xi)$  is the standard element of phase space, and  $M(\xi) = \sum_X A_X(\xi)$  is the matrix element describing the decay processes from the  $J/\psi$  to the final state  $\gamma 4\pi$ .  $A_X(\xi)$  is the amplitude corresponding to intermediate resonance  $X$ . We generate pseudo data sets with various signal strength  $\lambda = 0.001, \lambda = 0.003, \lambda = 0.005$ , and up to  $\lambda = 0.1$ . A pseudo-data set with  $\lambda = 0$  is also generated to verify the null case, where the pseudo-data and MC share the same model.

We perform anomaly detection using the classifier described in Sect. 3. The pseudo-data and MC samples are randomly split into  $2.5 \times 10^5$  events for training and  $2.5 \times 10^5$  events for testing. For each signal strength case, 50 random samplings of the data are performed. For each bootstrap method, 1000 bootstrap cycles are conducted. The confidence level for all tests is set at 95% ( $\alpha=0.05$ ). Table 4 shows the rate at which each test rejects the null hypothesis that no signal is present.

**Table 4** Rejection rate of the null hypothesis (no signal) for different signal strengths.

Test Statistic	Signal Strength ( $\lambda$ )						
	0.1	0.05	0.03	0.01	0.005	0	
Case 1 AUC	100	100	98	56	38	36	
Case 1 LRT	100	100	94	50	32	28	
Case 2 AUC	100	88	74	48	46	40	
Case 2 LRT	100	88	70	48	46	30	

Figure 2 shows the empirical distributions of the p-values produced by the classifier tests for different signal strengths. The cumulative distribution functions (CDFs) in the null case are approximately uniformly distributed, indicating good control of false-positive errors. In this demonstration with the amplitude analysis of  $J/\psi \rightarrow \gamma 4\pi$ , it is shown that the classifier is able to detect the contribution from an additional resonance with a signal strength of 0.01 in the tests of case 1 and case 2. The detection power is sufficient for practical amplitude analyses, where contributions with fit fractions larger than 1% are typically included in the nominal fit.

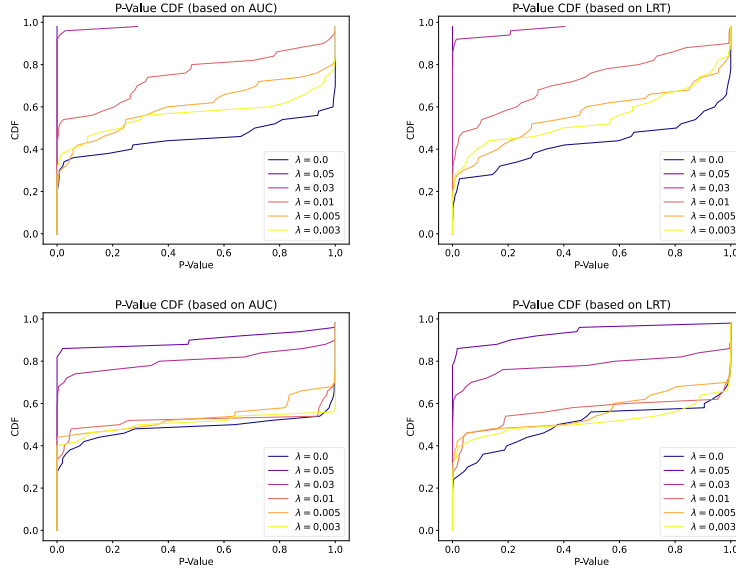


**Fig. 2** Empirical p-value distributions under varying signal strengths for additional resonances in (a)(b) Case 1 and (c)(d) Case 2. (a)(c) Using AUC statistic; (b)(d) Using LRT statistic. The dark blue line ( $\lambda = 0$ ) represents the null case.

## 5 Conclusion and outlook

Multivariate goodness-of-fit tests are essential for amplitude LRT analyses in hadron spectroscopy. We explore an ML-based anomaly detection method to evaluate goodness-of-fit for amplitude analyses of high-dimensional data. The performance study demonstrates the promise of this approach, which will be valuable for amplitude analyses of multi-body processes. Future work should incorporate systematic uncertainties when comparing amplitude analysis results to experimental data. For instance, systematic uncertainties in detection efficiency at the particle level can be addressed by reweighting the MC sample.

**Acknowledgements** This work is supported in part by National Natural Science Foundation of China (NSFC) under Contracts Nos.12235017, 12361141819; the Chinese Academy of Sciences Youth Team Program under Contract No. YSBR-101.

## Declaration

**Conflict of interest** On behalf of all authors, the corresponding author states that there is no conflict of interest.

## References

- [1] M. Battaglieri, B. J. Briscoe, A. Celentano, S. U. Chung, M. L. L. da Silva, A. D'Angelo, R. De Vita, M. Döring, J. Dudek and S. Eidelman, *et al.* Acta Phys. Polon. B **46**, 257 (2015).
- [2] Bellman, R. E. (1961). Adaptive Control Processes. Princeton University Press.
- [3] J. H. Friedman, eConf **C030908**, THPD002 (2003).
- [4] T. Chen and C. Guestrin, [arXiv:1603.02754 [cs.LG]].
- [5] M. Williams, JINST **5**, P09004 (2010).
- [6] C. Weisser and M. Williams, [arXiv:1612.07186 [physics.data-an]].
- [7] G. Claeskens and N. L. Hjort, Goodness of fit via non-parametric likelihood ratios, Scandinavian Journal of Statistics 31(4), 487 (2004).
- [8] P. Chakravarti, M. Kuusela, J. Lei and L. Wasserman, [arXiv:2102.07679 [stat.AP]].
- [9] E. M. Metodiev, B. Nachman and J. Thaler, JHEP **10**, 174 (2017).
- [10] B. S. Zou and D. V. Bugg, Eur. Phys. J. A **16**, 537-547 (2003).
- [11] J. Snoek, H. Larochelle and R. P. Adams, Advances in neural information processing systems **25** (2012).
- [12] P. I. Frazier, [arXiv:1807.02811].